PNAS RESEARCH ARTICLE | PHYSICS

Electro-nuclear quantum phase transition in $TmVO_4$

Mark P. Zic[a,b,1], Chao Huan[c,d], Nicolas Silva[c,d], Yuntian Li[a,e], Mark W. Meisel[c,d], and Ian R. Fisher[a,e,1]

Affiliations are included on p. 8.

Edited by J. C. Séamus Davis, University of Oxford, Oxford, United Kingdom; received November 27, 2025; accepted June 30, 2026

Hyperfine interactions couple nuclear and electronic degrees of freedom. The present work explores how hyperfine coupling within the Tm ions in $TmVO_4$ single crystals affects an electronic ferroquadrupole ordered ground state and its associated field-tuned quantum phase transition. As temperature is progressively reduced through the hyperfine energy scale, the nuclear moments reduce the critical field for the electronic order, resulting in a dramatic back-bending of the phase boundary delineating the ferroquadrupole order. This behavior is well described by a single-ion semiclassical mean-field model down to approximately 50 mK. Analysis of the effective Hamiltonian leads to a prediction of spontaneous nuclear magnetic order mediated by $4f$ electrons, which in principle persists with the application of orthogonal antisymmetric strain, yielding a proposed electro-nuclear tetracritical point.

quadrupole order | quantum phase transition | hyperfine interaction | electro-nuclear order | nematicity

Significance

Ferroquadrupole order is a local-moment realization of the wider class of electronic nematic order. A characteristic feature of nematic order is an associated ferroelastic phase transition, driven by bilinear coupling between the nematic order parameter and strain with the same symmetry. Here, for the specific case of $TmVO_4$, hyperfine interactions are shown to profoundly shape the phase boundary associated with ferroquadrupole order at low temperatures. For a specific range of temperatures and fields, the hyperfine interaction destabilizes ferroquadrupolar order; the nuclei drive a phase transition that affects the shape of the entire crystal lattice. This work also points to a previously unanticipated interplay between the observed electronic ferroquadrupolar order and a predicted ferromagnetic electro-nuclear order at even lower temperatures.

Quantum fluctuations, which arise as a consequence of noncommuting terms in an effective Hamiltonian, can drive a continuous quantum phase transition at zero temperature between states that are characterized by different symmetries (1, 2). Although the quantum critical point (QCP) occurs at $T = 0$, its effects can be felt at finite temperature, for example in terms of critical scaling exponents of various observable thermodynamic quantities. In experimental condensed matter physics, quantum critical points and phenomena have been posited in a wide variety of material systems, including structural, magnetic, superconducting, and various types of charge order. Hyperfine interactions couple nuclear and electronic degrees of freedom, implying that in the race toward $T = 0$, nuclear order and nuclear dynamics can also become entangled in the quantum critical state. Electro-nuclear quantum criticality has only been observed in a very small set of materials; principally $LiHoF_4$ (for which ferromagnetic order is tuned to a QCP by transverse magnetic fields) (3), $PrOs_4Sb_{12}$ (an antiferroquadrupolar material, also tuned by magnetic fields) (4), and $YbCu_{4.6}Au_{0.4}$ (a magnetically frustrated system that is characterized by electro-nuclear fluctuations in its ground state) (5). Here, we examine the case of an electro-nuclear quantum phase transition associated with ferroquadrupolar order. Because electronic ferroquadrupole order is necessarily accompanied by a complete softening of the crystal lattice in one symmetry channel [i.e., elastic quantum criticality (6)], the quantum phase transition is characterized by elastic, electronic, and nuclear quantum fluctuations, an incredible concatenation of fluctuations across enormous differences in microscopic length scales, all acting in sympathy. In addition, since the transverse field for ferroquadrupole order is a real magnetic field, the effect of hyperfine interactions is to cause an unusual back-bending of the phase boundary, which has interesting consequences affecting nuclear order in this material.

$TmVO_4$ is an insulator. The $J = 6$ Hund's rule ground state multiplet of the Tm ions are split by the crystal electric field (CEF), yielding a non-Kramers ground state doublet (7). The first excited state is 77 K above the ground state, so, at low temperatures the local electronic properties of each Tm ion can be described by a simple pseudospin representation (8, 9). Adding to the elegant simplicity of this material system, Thulium has a single (i.e., 100% abundance) naturally occurring, stable isotope, ^{169}Tm, with nuclear spin-1/2 (10). Thus, at low temperatures, the individual atomic electro-nuclear states in $TmVO_4$ can be effectively described by a simple four state Hamiltonian.

Bilinear coupling between electronic quadrupoles and lattice distortions of the same symmetry provides an effective interaction between local $4f$ electric quadrupoles. In $TmVO_4$, the dominant interaction between quadrupoles with an xy (B_{2g}) symmetry leads to ferroquadrupolar ordering with this symmetry at $T_Q = 2.15$ K via the Cooperative Jahn–Teller effect (8, 9). This ordering is accompanied by a spontaneous strain of the same symmetry, leading to a coincident structural distortion from tetragonal at high

Author contributions: M.P.Z. and I.R.F. designed research; M.P.Z., C.H., N.S., and Y.L. performed research; M.P.Z. and C.H. analyzed data; M.W.M. and I.R.F. advised and oversaw research; and M.P.Z., C.H., N.S., M.W.M., and I.R.F. wrote the paper.

The authors declare no competing interest.

This article is a PNAS Direct Submission.

[1]To whom correspondence may be addressed. Email: zic@alumni.stanford.edu or irfisher@stanford.edu.

This article contains supporting information online at https://www.pnas.org/lookup/suppl/doi:10.1073/pnas.2530567123/-/DCSupplemental.

Published July 22, 2026.

temperatures to orthorhombic in the ordered state (11). Within the framework of the pseudospin representation, a formal mapping to the transverse field Ising model can be made (12) in which the effective transverse fields for the pseudospins are a magnetic field along the crystallographic c-direction and orthogonal antisymmetric strain (i.e., induced strains with an $x^2 - y^2$, or B_{1g}, symmetry). Application of either of these effective transverse fields will suppress the long-range ferroquadrupole order (12).

The field-tuned phase diagram of $TmVO_4$ was determined down to ~500 mK in the 1970s via heat capacity (13) and radiofrequency susceptibility (14) measurements. Those data revealed a phase boundary that appeared to closely follow expectations for a simple semiclassical mean-field single-ion treatment of the transverse field Ising model (8). More recently, magnetocaloric effect (MCE) measurements down to 670 mK were used to reveal subtle deviations from this model toward low temperatures, which at the time were attributed to the effects of quantum critical fluctuations (15). As shown below, our present measurements reveal that this deviation, which becomes increasingly evident at yet lower temperatures, is actually associated with magnetic dipolar and hyperfine interactions.

Results

AC susceptibility measurements were used to follow the field-tuned phase transition in $TmVO_4$ down to 10 mK, one and a half orders of magnitude lower in temperature than previously observed. The specific advantage of susceptibility measurements is that the signature of the phase transition grows progressively larger at lower temperatures (*SI Appendix*), in contrast to heat capacity and MCE, which rely on entropy changes to mark the phase transition, and for which the signatures get progressively smaller in higher magnetic fields. Furthermore, AC susceptibility can be measured directly via mutual inductance, making this signature the ideal physical quantity to follow the field dependence of the phase transition. Two sets of experiments were performed on the same sample; one in a commercial Quantum Design dilution refrigerator insert at Stanford University (down to ~110 mK), and the other using an Oxford Instruments dilution refrigerator equipped with a homemade copper nuclear demagnetization stage in the High B/T facility of the National High Magnetic Field Laboratory at the University of Florida in Gainesville (down to 10 mK). In both cases, care was taken to ensure thermalization of the sample, and checks were performed to test for hysteresis. Due to the use of a mutual inductance technique, maximizing the filling factor of the coils was prioritized when selecting the sample, so a rectangular prism [3.616 mm (along c) × 0.958 mm (along a) × 0.467 mm (along a')] was used. Inhomogeneity of the internal field due to demagnetization effects within the nonellipsoidal sample yields a rounding of the jump in susceptibility at the phase transition. Quantitative modeling was not possible due to uncertainty in the field profile and the filling fraction of the sensing coils, but this effect does not preclude obtaining a sensitive measure of the critical field/temperature for the bulk of the sample. Experiments at Stanford were repeated for multiple samples to ensure reproducibility. Further details of the low temperature measurements are provided in *Materials and Methods*.

For small applied magnetic fields, the critical temperature does not change rapidly as the field is varied, and consequently the phase transition is most clearly seen in the magnetic susceptibility

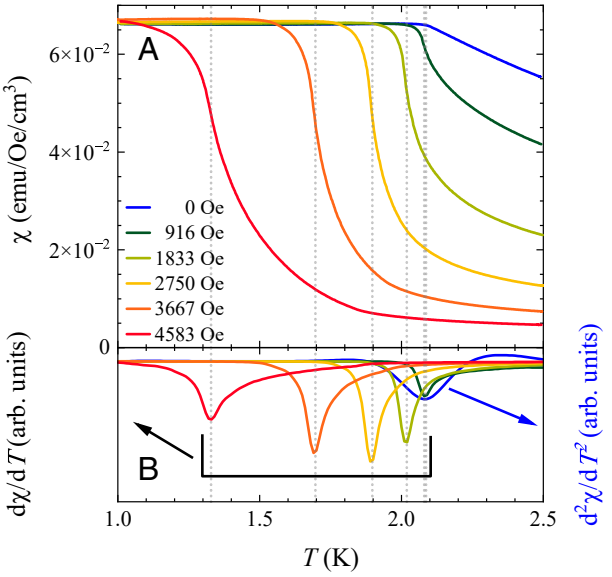

Fig. 1. Representative data showing the temperature dependence of (*A*) the magnetic susceptibility, and (*B*) the first derivative of the magnetic susceptibility, of $TmVO_4$ for different applied magnetic fields (second derivative for $H = 0$) (16). The field is applied along the crystalline c-axis, and acts as a transverse effective field for the ferroquadrupole order. As the magnetic field is increased in magnitude, the critical temperature for the ferroquadrupolar phase transition progressively decreases. The signature of the phase transition is also progressively broadened, which is tentatively ascribed to demagnetization effects, but the phase transition can still be identified by a minimum in the first derivative. For the specific case of zero field, a minimum in the second derivative marks the phase transition (see discussion in main text). Vertical gray dotted lines mark the phase transition.

via temperature sweeps at fixed field. In zero applied field, the magnetic susceptibility exhibits a sharp kink at $T_Q \approx 2.1$ K, shown in Fig. 1*A*. Below the critical temperature, the susceptibility is independent of temperature, dropping sharply as temperature is increased above T_Q. This behavior conforms to expectations of the single-ion mean-field model previously used to describe the properties of $TmVO_4$ (8); calculated curves are shown in *SI Appendix* for comparison. As the magnetic field is progressively increased, the critical temperature decreases. The phase transition is now marked by a sharp drop in the susceptibility (*SI Appendix*), which is progressively rounded due to the change in the distribution of internal fields. Motivated by calculations of the susceptibility for the mean-field model (*SI Appendix*), the minimum in the first derivative of the susceptibility with respect to temperature (shown in Fig. 1*B*) is used to estimate the critical temperature for nonzero values of the field, while the second derivative is used for the case of zero field. Vertical dashed lines in Fig. 1 show the critical temperature extracted from these methods. These values for the critical temperature as a function of field provide the high-temperature portion of the phase diagram.

For larger magnetic fields, the phase boundary becomes much steeper (i.e., the critical temperature varies much more rapidly with field), and consequently field sweeps at fixed temperature are used to map the rest of the phase diagram. Representative data measured from 800 mK down to 110 mK at Stanford University are shown in Fig. 2*A*; representative data measured from 200 mK down to 10 mK in the MagLab High B/T facility at the University of Florida are shown in Fig. 2*B*. The phase transition is marked by a downward step in the susceptibility (*SI Appendix*). This downward step is somewhat rounded in the experiment, presumably due to the anticipated field inhomogeneity within the

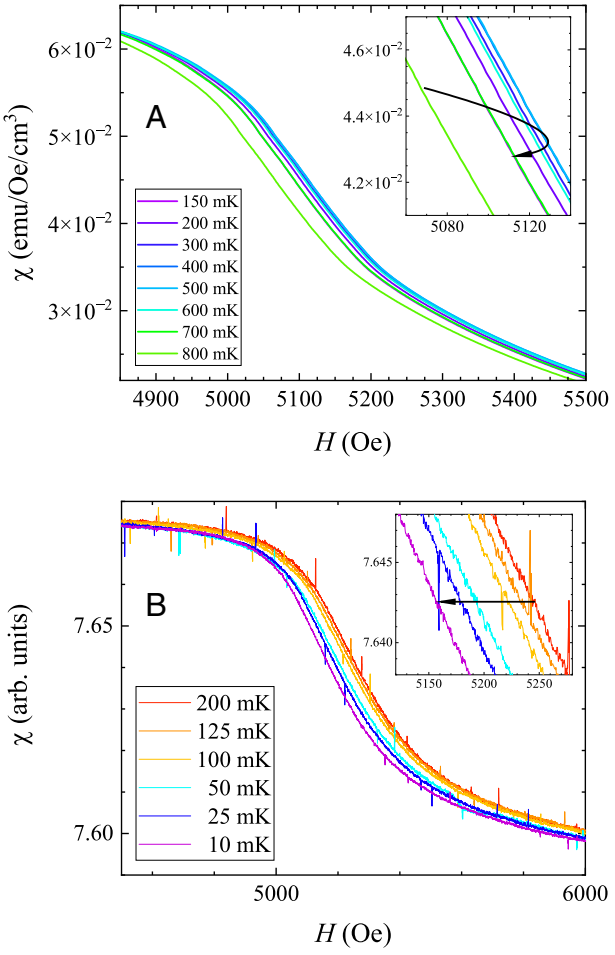

Fig. 2. Representative data showing the field dependence of the magnetic susceptibility of $TmVO_4$ at different temperatures using (*A*) a dilution refrigerator at Stanford University for the temperature range from 800 mK down to 110 mK, and (*B*) a dilution refrigerator at the High B/T Laboratory for the temperature range from 200 mK down to 10 mK (16). The critical field is marked by a drop in the susceptibility (see discussion in main text). In panel (*A*), the critical field exhibits nonmonotonic behavior, initially increasing as temperature is reduced from 800 mK, before starting to decrease as the temperature is reduced below 500 mK. In panel (*B*), where data were taken to even lower temperatures, the critical field monotonically decreases, but with a rate that varies with the field. Inserts to both panels show near the midpoint of the transition in each case on an expanded scale, and include arrows that point from high temperatures toward lower temperatures.

sample arising from demagnetization effects, though as remarked earlier, quantitative analysis of the broadening is not possible due to uncertainty in the field profile and filling factor of the sensing coils. For sufficiently slow sweeps up/down in field, the data do not exhibit hysteresis, and the phase transition appears to remain continuous.

Insets to Fig. 2 show expanded views near the midpoint of the phase transition. Inspection of these figures reveals a remarkable nonmonotonic behavior of the critical field. Considering first Fig. 2*A*, the critical field steadily increases as the temperature is progressively reduced from 800 mK down to 500 mK. However, below approximately 450 mK the critical field starts to decrease with further reduction in temperature (indicated by the curved arrow in the *Inset*). Data shown in the *Inset* to Fig. 2*B* indicate that this reduction in the critical field continues down to 10 mK.

Within the mean-field model, the phase transition is marked by a discontinuity in the susceptibility as a function of field (*SI Appendix*), and hence the minimum in the first derivative with respect to field provides the best measure of the critical field and was used to extract values from the present data. Representative data are shown in *SI Appendix*.

Piecing together critical temperature and critical field values from the field sweeps and temperature sweeps respectively, yields the phase diagram shown in Fig. 3. A remarkable back-bending of the phase boundary is clearly observed as the temperature is reduced below 500 mK. Quantitative analysis (see below) indicates this behavior arises from the hyperfine interaction within the Tm ions.

Discussion

Mean-Field Description. As mentioned previously, mean-field models have been commonly used to understand the spin interactions in $TmVO_4$, but now hyperfine interactions are explicitly included to frame our discussion of the experimental phase diagram. Specifically, $TmVO_4$ can be described by a transverse field Ising model Hamiltonian in which the *xy*-symmetric quadrupoles are represented by spin matrices in one direction (S^y here), $x^2 - y^2$-symmetric quadrupoles are represented by spin matrices in another direction (S^x here), and the magnetic dipoles are represented by spin matrices in the third transverse direction (S^z here) (8, 9, 12). The choice of which spin matrix to associate with which symmetry electronic state (*xy* quadrupole, $x^2 - y^2$ quadrupole, *z*-axis magnetic dipole) is not important as long as the choice remains consistent (8, 9). Here, to avoid confusion, the magnetic dipole is specifically chosen to be described by the *z*-component of the pseudospin, so that the effective field for the *z*-axis component of the pseudospin corresponds to a real *z*-axis magnetic field. Hyperfine coupling links the electronic and nuclear degrees of freedom, but the strong magnetic anisotropy ($g_a \approx 0$ due to the non-Kramers nature of the CEF eigenstate) means that only the *z* component of nuclear moment interacts with the electronic dipole moment. The Hamiltonian that we consider, in its most general form, is then:

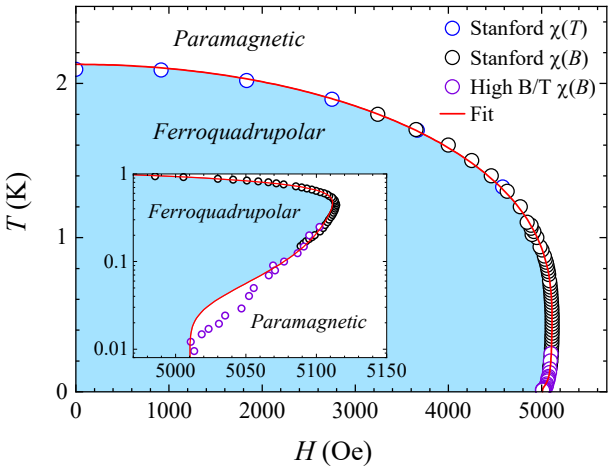

Fig. 3. Phase diagram of $TmVO_4$ as a function of applied magnetic field (16). Ferroquadrupole order is shown by blue shading. The influence of the hyperfine coupling of the electrons to the Tm nucleus is especially apparent below approximately 500 mK, where back bending of the phase boundary begins. The fit to Eq. **2**, which describes the single-ion semiclassical mean-field model that includes hyperfine interactions, is shown by the red line, with fit parameters given in the main text. *Inset* shows the same data on a log–linear scale to more clearly reveal the remarkable back-bending of the phase boundary.

$$H = -\frac{1}{2}\sum_{\langle i,j\rangle} J^y_{ij} S^y_i S^y_j - \Gamma^z \sum_i S^z_i - \Gamma^x \sum_i S^x_i - \frac{1}{2}\sum_{\langle i,j\rangle} J^z_{ij} S^z_i S^z_j - A^z \sum_i I^z_i S^z_i. \quad [1]$$

Here, J^y is the quadrupolar coupling; the transverse effective field Γ^z is $\frac{1}{2}g_c\mu_B B_z$, where B_z is a magnetic field oriented along the crystallographic c-axis; the transverse effective field Γ^x is $\eta_{x^2-y^2}\varepsilon_{x^2-y^2}$, where $\eta_{x^2-y^2}$ is the magnetoelastic coupling for the orthogonal antisymmetric strain $\varepsilon_{x^2-y^2}$; J^z is the dipolar coupling; and A^z couples the nuclear spin (I^z) to the electronic spin (S^z). It is the last term in this Hamiltonian, the hyperfine coupling to the Tm nucleus, that is imperative in understanding the low temperature behavior of $TmVO_4$ uncovered in this work.

To model the data, the Hamiltonian is simplified considerably to a mean-field, single-ion, semiclassical model. This Hamiltonian takes the form (*SI Appendix*):

$$H_{mf} = -J^y\langle S^y\rangle S^y + \left(-\Gamma^z - J^z\langle S^z\rangle - A^z\langle I^z\rangle\right)S^z - \Gamma^x S^x - A^z\langle S^z\rangle I^z. \quad [2]$$

Inspection of Eq. **2** clearly reveals that both the dipolar interaction and the hyperfine coupling effectively strengthen the effects of the transverse field (i.e., the effective transverse field seen by the pseudospin is $(\Gamma^z + J^z\langle S^z\rangle + A^z\langle I^z\rangle)$), which will reduce the applied field necessary to suppress the quadrupolar order. Treated at this mean-field level, however, these two terms act in slightly different ways. In the absence of hyperfine interactions, in the ferroquadrupole ordered phase, $\langle S^z\rangle$ is constant as a function of temperature for fixed field (a property of the transverse field Ising model). This term serves only to renormalize the effective field by a constant factor, independent of temperature, and thus does not change the functional form of the phase boundary. In contrast, the hyperfine interaction introduces an additional degree of freedom, the nuclear moment, and consequently the shape of the phase boundary is affected upon cooling through this energy scale. In this regime, the nuclear hyperfine field experienced by the electronic state progressively enhances the external field, and thus, the critical applied field that is required to destabilize the ferroquadrupole order is reduced. Ultimately, the observable consequence is that the phase diagram will exhibit "back-bending."

Fits to the Mean-Field Model. In the absence of transverse (orthogonal antisymmetric) strains (i.e., $\Gamma^x = 0$), the above mean-field model contains only four free parameters: the mean-field coupling between quadrupoles, J^y; the g-factor g_c (where $\Gamma^z = \frac{1}{2}g_c\mu_B B_z$); the mean-field coupling between magnetic dipoles J^z, and the hyperfine scale A^z. In practice, all four of these quantities can be independently determined, but initially each one was treated as a fitting parameter that was varied to obtain the best fit to the observed phase boundary.

The best fit to the data (shown by the red line in Fig. 3) yields the parameters $J^y = 2.12 \pm 0.04$ K, $g_c = 11.44 \pm 0.24$, $J^z = 0.16 \pm 0.08$ K, and $A^z = 43.4 \pm 5.7$ mK. The coupling strength J^y agrees with the zero-field critical temperature, observed here via susceptibility measurements, and in agreement with heat capacity data [$T_Q = 2.15$ K (17)]. The value for g_c is not in perfect agreement with previous optical measurements [$g_c = 10.21 \pm 0.15$ (18)], but we note that it is significantly closer in value to more recent measurements based on precise ultrasound attenuation measurements in $Tm_{0.03}Y_{0.97}VO_4$, [$g_c = 11.8$ (19)]. The mean-field magnetic interaction J^z closely agrees with the Weiss temperature extracted from separate longitudinal magnetic susceptibility measurements (*SI Appendix*). Finally, the hyperfine coupling is within one SD of the value recently obtained from ultrasound attenuation measurements [46.5 mK (19)]. Thus, all the fit parameters are in good agreement with values that can be obtained from other, independent, measurements.

Inspection of Fig. 3 reveals that for temperatures above 50 mK the semiclassical single-ion mean-field model provides a remarkably good description of the phase boundary of $TmVO_4$. The quality of fit, combined with the physically reasonable fit parameters obtained, implies that the origin of the observed back-bending is indeed due to hyperfine interactions. This is the major result of the present study. We discuss the specific significance of this observation below, but first comment on apparent deviations from the mean-field model below 50 mK.

Low Temperature Deviations from the Mean-Field Model. The single ion semiclassical mean-field model provides a remarkably good description of the data from the zero-field critical temperature at 2.15 K all the way down to 50 mK, and therefore seems to capture all the essential physics in this wide temperature regime. Nevertheless, inspection of the *Inset* to Fig. 3 reveals a deviation between the data and the best fit to the mean-field model below approximately 50 mK. In the absence of any known source of systematic experimental uncertainty, this appears to point to additional physics not captured in the single-ion semiclassical mean-field model below approximately 50 mK. However, investigation of systematic uncertainties associated with fitting to the associated model (*SI Appendix*) reveals that the fit parameters can vary by small amounts depending on the fitting range, the estimated error in each data point, and even on the starting values used to initiate the regression. Hence, the residuals between the best fit and the data cannot be used with any confidence to estimate the functional form of any additional effect.

Two pieces of physics that are explicitly absent from the model are the effects of quantum fluctuations and of hyperfine interactions on the V ions. The model also assumes that the magnetic interactions can be adequately treated at a mean-field level. Measurements to approximately a decade lower in temperature will be necessary to fully quench the Tm hyperfine interaction in order to address this.

Quantum Criticality. Since the phase transition in $TmVO_4$ remains continuous down to the lowest temperatures measured, quantum critical fluctuations are anticipated upon approaching the quantum phase transition. The thermal phase transition for Ising nematic order is mean-field-like due to the long-range nematic interaction generated by the coupling to acoustic phonons (6, 20, 21). Since the thermal phase transition is mean-field-like, the QCP should also be. For an insulator with strong nemato-elastic coupling, theoretical work predicts a phase boundary possessing a power law dependence, $T_Q \sim (H_c^0 - H_c)^\psi$ (15), where H_c^0 is the critical field at zero temperature, and ψ is given by the standard scaling relation $\psi = z/(z + d - 2)$ (22). The effective dimensionality, d, is 5 because the correlation length only diverges along specific directions (6). As described in ref. 15, the softening of acoustic phonons, which affects the phonon dispersion near zero frequency, means that the dynamical critical exponent z, which characterizes temporal fluctuations of the order parameter near the QCP, will vary from a value of 1 at higher temperatures, to a value of 2 at lower temperatures.

The electro-nuclear effects revealed in the present study significantly complicate efforts to observe this anticipated power-law behavior. Indeed, since the phase boundary can be adequately described down to ∼50 mK by the semiclassical result, which neglects quantum fluctuations of the order parameter, one may conclude either 1) that the quantum critical dynamics do not manifest until significantly below this temperature; or 2) that the progressive effect of hyperfine interactions (and possibly also dipolar and exchange interactions if these act in a non-mean-field way) dwarfs any more subtle effects associated with growing quantum critical fluctuations, at least in the range of temperatures considered here. Either way, experiments to yet lower temperatures will be required, in order to freeze out any temperature dependence associated with the hyperfine interaction. The mean-field model developed here indicates that below approximately 10 mK, the phase boundary will cease back-bending, providing an upper bound below which subsequent measurements should test for the theoretically predicted power law behavior of the phase boundary. This is also true of other physical quantities for which quantum fluctuations are anticipated to yield power laws, including the longitudinal susceptibility, motivating a concerted effort to study this material in the sub-mK regime.

Unique Aspects of the Electro-Nuclear Effects in $TmVO_4$. With our observations, $TmVO_4$ joins only a handful of other materials for which nuclear interactions have been shown to play an important role in the electronic order and/or quantum phase transition, including $LiHoF_4$ (3, 23–25), $PrOs_4Sb_{12}$ (4), $YbCu_{4.6}Au_{0.4}$ (5), $YbRh_2Si_2$ (26–28), $PrCu_2$ (29), and $Pr_3Pd_{20}Ge_6$ (30, 31).

Of these materials, $LiHoF_4$ provides a particularly insightful point of comparison for $TmVO_4$. Both materials are tetragonal, though with different crystal structures. The magnetic ion in both cases has the same symmetry non-Kramers CEF doublet ground state (i.e., belongs to the same irreducible representation of the point group), which can harbor a c-axis magnetic dipole and the two in-plane quadrupoles (with $x^2 - y^2$ and xy symmetry). As described above, $TmVO_4$ is an Ising quadrupolar system, with long-range quadrupolar interactions. $LiHoF_4$, however, orders via its dipole moment, and is an Ising ferromagnet with long-range dipolar interactions. The thermal phase transitions in both materials are of interest: The Ising model with long-range strain interactions has an upper critical dimension $d^+ = 2$ (6), so the phase transition in $TmVO_4$ is mean-field-like (13), whereas $d^+ = 3$ for the Ising model with long range dipolar interactions, such that $LiHoF_4$ exhibits marginal dimensionality (32). Both systems can be mapped onto a variant of the transverse field Ising model, with an in-plane magnetic field (H_x^2) acting as the transverse field for $LiHoF_4$ (3), and a c-axis magnetic field (H_z) acting as the transverse field for $TmVO_4$. Both nuclei, Ho and Tm are 100% abundant with a single isotope, though they differ in the nuclear spin, with Tm having the simplest case of $I = 1/2$. Hyperfine interactions in $LiHoF_4$ serve to strengthen the ferromagnetic order, such that the field-tuned phase boundary extends further than if there were no hyperfine interactions (3); whereas the hyperfine interactions in $TmVO_4$ enhance the effect of the transverse field, leading to the "back-bending" of the phase boundary shown in Fig. 3. The two materials, $TmVO_4$ and $LiHoF_4$, are compared in Table 1; both are model systems for studying thermal and quantum phase transitions in the context of hyperfine interactions, exhibiting sufficient complexity to be interesting, but sufficient simplicity to be tractable (from both experimental and theoretical perspectives).

The fascinating effects of hyperfine interactions on quantum criticality have been discussed for a range of electronic states (33), but to our knowledge the case of quadrupolar order has thus far been neglected. The backbending of the phase boundary that we observe for $TmVO_4$ reveals a regime in which, for approximately 2 decades of temperature (from approximately 1 K down to 10 mK, and for fields in the range from approximately 5,000 Oe to 5,200 Oe), the progressive effects of the hyperfine interaction destabilize the electronic order. Since the quadrupole order determines the spontaneous strain state of the crystal lattice, the Tm nuclei indirectly impact the macroscopic shape of the crystal lattice in this broad regime of field and temperature, a remarkable effect considering the physical size of the microscopic nuclei relative to the macroscopic crystal.

The back-bending of the phase boundary also implies that adiabatic demagnetization in this regime would result in a cooling effect (*SI Appendix*). While nuclear adiabatic demagnetization is a commonly used technique, here the effect could be usefully employed to further confirm the entropy landscape that the mean-field model predicts.

Finally, we discuss below in somewhat greater detail one final aspect of hyperfine interactions in $TmVO_4$ that makes this specific case especially interesting to study in some detail; the interaction of the electronic quadrupolar order with an anticipated low-temperature electro-nuclear ferromagnetic state.

Implications for Nuclear Order. Nuclear moments are considerably smaller than electronic ones, with the ratio of the nuclear and Bohr magnetons being $\mu_N/\mu_B = m_e/m_p$ where m_e and m_p are the mass of the electron and proton respectively. Nevertheless, nuclear order can occur at a substantially elevated temperature relative to that which would be anticipated if the nuclear moments interact solely through their dipolar fields. When electronic magnetic order exists, hyperfine interactions necessarily split any nuclear degeneracy and lead to an induced nuclear moment on these ions, precluding spontaneous nuclear magnetic order. However, for van Vleck materials, which have a singlet CEF ground state but an enhanced paramagnetic susceptibility due to the presence of low-lying CEF excited states, the nuclear degeneracy can be lifted through spontaneous nuclear magnetic order, with the nuclear moments coupled via the electronic system (34). In these systems, the hyperfine interaction enables the nuclear moment to co-opt some small amount of $4f$

Table 1. Comparison between $TmVO_4$ and $LiHoF_4$

Material	Active ion	Ordering	T_c	I	J	$N_{H_{MF}}$
$TmVO_4$	Tm^{3+}	Ising ferroquadrupolar	2.15	1/2	6	4
$LiHoF_4$	Ho^{3+}	Ising ferromagnet	1.53	7/2	8	136

The active ions, ordering, transition temperature, nuclear spin I, electronic total angular momentum J, and the size of the mean-field matrix $N_{H_{mf}}$ are listed for both materials. Note that, given the nature of the crystal field eigenstates and the transverse fields for each material, the Hamiltonian used to model $TmVO_4$ is of much lower rank, greatly adding to its appeal as a model system to study quantum phase transitions.

dipole moment on each ion, leading to an enhanced effective nuclear moment, $\mu = g_N \mu_N (1+K)\langle I \rangle$, where g_N is the nuclear g-factor and K is an element and material specific enhancement factor. Examples include the intermetallic compounds $PrCu_2$ (35), $PrCu_6$ (36), $PrNi_5$ (37), and the insulator $HoVO_4$ (38) (which belongs to the same crystal structure as $TmVO_4$). The absence of magnetic order in $TmVO_4$ (which, courtesy of the quadrupolar order, renders itself a van Vleck magnet below T_Q) makes this material a natural candidate for nuclear magnetic order. The key difference to all other known van Vleck nuclear magnets is that the splitting of the CEF states in $TmVO_4$ is not caused by the crystal symmetry, but rather is induced by the quadrupolar phase transition, and therefore can be modulated by the material in order to minimize the free energy; in other words, the quadrupolar order parameter can interact with the electro-nuclear order. In the pseudospin language, the electronic pseudospin can spontaneously rotate on its Bloch sphere, moving away from the pure quadrupole "direction" in order to acquire some small dipole moment. This leads us to propose an interplay between the nuclear and quadrupolar order in this material at very low, but hopefully accessible, temperatures.

In the case of $TmVO_4$, the enhancement factor $(1 + K)$ for the Tm ion was previously estimated to have a value of 774 (14, 39), indicating the possibility of nuclear magnetic order at an elevated temperature. Bleaney and Wells estimated a critical temperature based on calculations of the nearest neighbor dipole–dipole interactions, finding that ferromagnetic order is favored with an estimated critical temperature of 0.25 mK (14). They noted that a small amount of superexchange interaction could favor an antiferromagnetic state, estimating in that case a critical temperature of 0.28 mK based on estimates of the induced field on the V nuclei (14). Including exchange interactions within the mean-field model developed herein, and using the same values for the fit parameters described above, a nonzero expectation value of the nuclear order parameter at zero temperature, and, for zero applied magnetic field, a phase transition to a ferromagnetically ordered state deep within the ferroquadrupole state, is also found. Based solely on the fit parameters obtained from the phase diagram, which indicate a dominant ferromagnetic coupling between Tm dipole moments, we obtain a somewhat higher predicted mean-field critical temperature than Bleaney and Wells, $T_{mf} = (A^z)^2/(J^y - J^z) = 0.96$ mK (*SI Appendix*). Despite these predictions, nuclear demagnetization experiments performed on $TmVO_4$ by Suzuki et al. in 1980 found no evidence for magnetic order down to 0.1 mK (39), indicating the presence of frustration of one sort or another, potentially reflecting the competing effects of superexchange and dipolar interactions. In the following analysis, we use the calculated mean-field critical temperature T_{mf} in order to make a couple of important symmetry-related points (i.e., conclusions that do not depend on microscopic details, but only on the symmetry of the ordered state), while noting that the actual critical temperature is clearly somewhat lower in temperature.

First, if the nuclear order is indeed ferromagnetic (as the observed Weiss temperature implies) then in the presence of a nonzero magnetic field there will be no spontaneous phase transition since time-reversal symmetry is already broken by the magnetic field (Fig. 4*A*). Consequently, the complete phase diagram for $TmVO_4$ as a function of magnetic field would comprise the ferroquadrupole ordered state and a single critical point for the ferromagnetic electro-nuclear order. This is illustrated in Fig. 4*B*, in which the predicted mean-field critical point for the ferromagnetic order T_{mf} is shown by a star. For comparison, a heat map of $\langle I^z \rangle$ is overlaid, demonstrating that a nonzero magnetic field smears out the phase transition and graphically illustrating how the observed "back-bending" of the phase diagram coincides with the growing nuclear moment as temperature is reduced below approximately 500 mK.

While the field-tuned phase diagram is hardly modified by the nuclear order, having only a single critical point in zero magnetic field, the predicted strain-tuned phase diagram is significantly richer. As mentioned above, orthogonal antisymmetric strain $\varepsilon_{x^2-y^2} = \varepsilon_{xx} - \varepsilon_{yy}$ is also a transverse effective field for the xy symmetry quadrupole order. Since strain does not break time reversal symmetry, spontaneous nuclear ferromagnetic order is still allowed, and hence the electro-nuclear order persists across the entire phase diagram. Fig. 4 *C* and *D* show the results of the mean-field model for $\langle I^z \rangle$ and the associated phase diagram. The mean-field theory predicts an electro-nuclear tetracritical point, in which the purely electronic quadrupolar phase boundary crosses the electro-nuclear ferromagnetic phase boundary. As temperature is decreased below the tetracritical point, the quadrupolar phase boundary exhibits a subtle back-bending (shown on an expanded scale in the *Inset* to Fig. 4*D*). In the ferromagnetic phase, the pseudospin describing the electronic quadrupole rotates slightly to acquire some small amount of magnetic dipole moment. In so doing, the critical strain to suppress the quadrupole order is reduced, leading to the back-bending. Below this temperature, the two coexisting orders are remarkably intertwined, since the electronic states contribute to both the electronic quadrupole order and the electro-nuclear ferromagnetism. Finally, the ferromagnetic order is predicted to persist for strains beyond the critical strain for the quadrupole order (i.e., for strains beyond approximately $2 \cdot 10^{-3}$), but the critical temperature grows progressively smaller with increasing strain as the strain-induced splitting of the CEF doublet grows progressively larger.

Although earlier experiments indicate that the nuclear order in $TmVO_4$ occurs at a lower temperature than the mean-field estimate calculated in this work, nevertheless it is inevitable that the nuclear moments will eventually order, and the large enhancement factor K implies a relatively high critical temperature. Our theoretical predictions motivate performing the challenging experiments that will be necessary to explore the remarkable phase diagram predicted in Fig. 4*D* and further motivate studying this fascinating material in the sub-mK regime.

Materials and Methods

Crystal Growth. Measurements were performed on a sample of $TmVO_4$ shaped as a rectangular prism with dimensions 3.616 mm (along the crystallographic *c*-axis) by 0.958 mm (along the crystallographic *a*-axis) by 0.467 mm (along the orthogonal *a*-axis). The sample was grown using a flux growth method (15, 40, 41) and subsequently cleaned, cut with a wire saw, and polished using fine sandpaper.

AC Susceptibility Measurements. AC magnetic susceptibility measurements were performed at both Stanford University and the National High Magnetic Field Laboratory (MagLab) High B/T Facility at the University of Florida. Measurements at Stanford University were performed using a commercial Quantum Design DynaCool with a dilution refrigerator insert, using a field amplitude of 3 Oe and a frequency of 643 Hz. No frequency dependence was observed in the range tested (approximately 100 to 1,000 Hz).

Measurements at the MagLab High B/T Facility were performed using a homemade ultralow temperature AC susceptometer, which allowed the sample

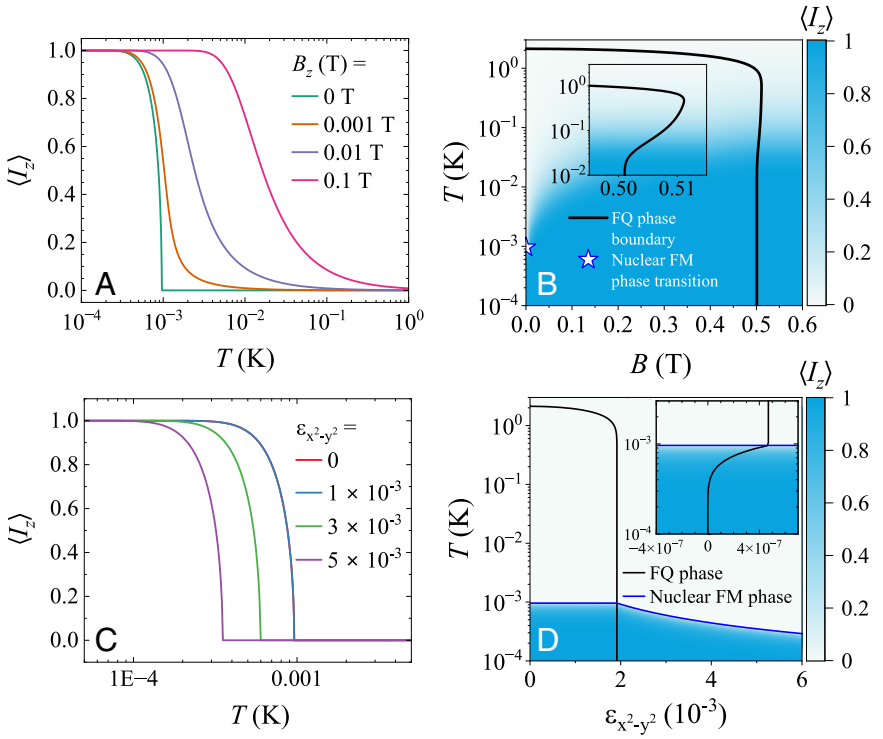

Fig. 4. Predictions for nuclear order in $TmVO_4$ based on the mean-field model, as a function of the two transverse effective fields (16). The temperature dependence of the nuclear order parameter $\langle I_z \rangle$ for different values of applied magnetic field is shown in panel (*A*) with associated phase diagram in panel (*B*), while temperature dependence of the nuclear order parameter $\langle I_z \rangle$ for different values of applied strain $\epsilon_{x^2-y^2}$ is shown in panel (*C*) with associated phase diagram in panel (*D*). The associated phase diagrams are shown in panels (*B* and *D*), together with a heat map (blue color scale) of the nuclear order parameter. In both figures, the ferroquadrupolar phase boundary is depicted by a solid black line. In panel (*B*), the nuclear ferromagnetic phase transition predicted by this mean-field model (see discussion in main text) occurs at approximately 0.96 mK and is marked by a blue star. The phase transition only occurs in zero field, and is smeared out for nonzero values of *B*. The expectation value of the nuclear spin operator begins to grow at higher temperatures as field is progressively increased, directly affecting the shape of the phase boundary; the temperature at which the phase boundary "back-bends" corresponds to the temperature at which the nuclear moment starts to grow rapidly (shown on an expanded scale in the *Inset*). In panel (*D*), the solid blue line corresponds to the nuclear ferromagnetic phase transition, which persists as a function of strain. *Inset* shows an expanded scale close to the predicted tetracritical point (see discussion in main text).

to be entirely immersed in liquid ^{3}He thermalized by a silver sinter heat exchanger, mounted on the Bay 2 instrument, using a field amplitude of 0.01 Oe and a frequency of 106.7 Hz. The lower frequency and amplitude used at the MagLab High B/T Facility were chosen to reduce heating effects at low temperatures. In both cases (i.e., measurements performed at Stanford and at the MagLab) data are reported for the lowest sweep rates (to minimize heating in metallic components of the fridges), and all measurements were performed upon decreasing the magnetic field from fields greater than the critical field. The reported temperature values of the sample are based on thermometry provided by a ^{3}He melting curve thermometer (MCT) mounted on top of the nuclear stage of the refrigerator system. To verify that the MCT reading accurately reflected the thermodynamic temperature of the pure liquid ^{3}He in the immersion cell, a calibration against a quartz-tuning-fork thermometer positioned in that cell was performed. Over the temperature interval relevant to the data (2 mK to 200 mK) the two thermometers agreed to within 1 mK; the maximum offset observed was ∼1.5 mK at ∼100 mK. Below 100 mK the deviation falls well below 1 mK. Consequently, the systematic temperature uncertainty is far smaller than the symbol size used in the figures. The sample temperature was allowed to equilibrate with the liquid ^{3}He before the acquisition of data. After every temperature change, data collection was paused for approximately five hours, a duration chosen to exceed by a factor of five the intrinsic thermal relaxation time of the entire assembly. As shown in ref. 42, the hyperfine interaction enhanced nuclear dipole interaction between Tm and ^{3}He is strong, which can significantly decrease the boundary thermal resistance. For a powdered $TmVO_4$ sample immersed in liquid ^{3}He, the thermal relaxation time is shorter than 1 min when the temperature is above 1 mK.

To stitch the critical field measurements from both facilities together, measurements were performed in an overlap region (roughly 110 mK to 200 mK). A reduction of approximately 1% was applied to the critical fields measured at the MagLab High B/T Facility to yield good stitching, which presumably accounts for mismatches in sampling alignment/mounting, slight imperfections in the crystal during shipping/handling that changed its demagnetizing fields, and any other sample/instrument calibration mismatches between the two facilities.

Several attempts were made to obtain reasonable uncertainty values for the critical temperatures and critical fields used to establish the phase boundary as shown in Fig. 3 in the main text. However, the uncertainties obtained arising from the data analysis alone were very small (i.e., the methods of extracting the critical temperature/field were very precise), usually orders of magnitude smaller than the temperature/field points themselves. The temperature and field setpoints were also very stable in the regimes measured, yielding similarly small uncertainties. There are other possible sources of uncertainty, such as systematic uncertainties from the field inhomogeneity of the sample, or random uncertainties from temperature fluctuations from the magnetocaloric effect of $TmVO_4$, among others. For the purposes of obtaining reasonable uncertainties for the fit parameters to the mean-field model of the phase boundary, a heuristic temperature uncertainty of 2% of the temperature setpoint was used as well as a heuristic magnetic field uncertainty of 25 Oe was used. It is important to stress that if the very small uncertainties were used for the temperature/field points in the phase boundary, the uncertainties reported for the fit parameters would be unnecessarily large and effectively meaningless. It is noteworthy that the values for the uncertainties only manifest as minor changes in the values of the fit parameters, and the overall effects of the hyperfine interaction on the shape of the phase diagram in $TmVO_4$ remain consistent.

Data, Materials, and Software Availability. Numeric data have been deposited in Stanford Digital Repository (https://purl.stanford.edu/ky369kj8044) (16). All other data are included in the manuscript and/or *SI Appendix*.

ACKNOWLEDGMENTS. We thank N. Curro, R. Fernandes, P. Hollister (who first pointed out the possible effects of hyperfine interactions on the ground state of $TmVO_4$), J. Hu, S. A. Kivelson, D. Petruzzi, and B. J. Ramshaw for helpful conversations. Crystal growth and low temperature susceptibility measurements performed at Stanford were supported by The Air Force Office of Scientific Research under award FA9550-20-1-0252 and award number FA9550-24-1-0357; data taken at Stanford were obtained using a cryostat acquired with award FA9550-22-1-0084. The work at the University of Florida and High B/T Facility, as a part of the National High Magnetic Field Laboratory (MagLab), was supported by the NSF through NSF/DMR-2128556 and the state of Florida. M.P.Z. was partially supported by a NSF Graduate Research Fellowship under award DGE-1656518.

Author affiliations: [a]Geballe Laboratory for Advanced Materials, Stanford University, Stanford, CA 94305; [b]Department of Physics, Stanford University, Stanford, CA 94305; [c]Department of Physics, University of Florida, Gainesville, FL 32611; [d]National High Magnetic Field Laboratory High B/T Facility, University of Florida, Gainesville, FL 32611; and [e]Department of Applied Physics, Stanford University, Stanford, CA 94305

1. J. A. Hertz, Quantum critical phenomena. *Phys. Rev. B* **14**, 1165–1184 (1976).
2. S. Sachdev, *Quantum Phase Transitions* (Cambridge University Press, 2000).
3. D. Bitko, T. F. Rosenbaum, G. Aeppli, Quantum critical behavior for a model magnet. *Phys. Rev. Lett.* **77**, 940–943 (1996).
4. F. Bangma *et al*., Diverse influences of hyperfine interactions on strongly correlated electron states. arXiv [Preprint] (2023). https://arxiv.org/abs/2305.17088 (Accessed 9 February 2025).
5. J. Banda *et al*., Electronuclear quantum criticality. arXiv [Preprint] (2023). https://arxiv.org/abs/2308.15294 (Accessed 9 February 2025).
6. I. Paul, M. Garst, Lattice effects on nematic quantum criticality in metals. *Phys. Rev. Lett.* **118**, 227601 (2017).
7. K. D. Knoll, Absorption and Fluorescence Spectra of Tm^{3+} in YVO_4 and YPO_4 *Phys. Status Solidi B* **45**, 553–559 (1971).
8. R. Melcher, 1 - The anomalous elastic properties of materials undergoing cooperative Jahn-Teller phase transitions. *Phys. Acoust.* **12**, 1–77 (1976).
9. G. A. Gehring, K. A. Gehring, Co-operative Jahn-Teller effects. *Reports Prog. Phys.* **38**, 1–89 (1975).
10. F. Kondev, M. Wang, W. Huang, S. Naimi, G. Audi, The nubase2020 evaluation of nuclear physics properties*. *Chin. Phys. C* **45**, 030001 (2021).
11. A. Segmüller, R. Melcher, H. Kinder, X-ray diffraction measurement of the Jahn-Teller distortion in $TmVO_4$. *Solid State Commun.* **15**, 101–104 (1974).
12. A. V. Maharaj *et al*., Transverse fields to tune an Ising-nematic quantum phase transition. *Proc. Natl. Acad. Sci. U.S.A.* **114**, 13430–13434 (2017).
13. A. Cooke, S. Swithenby, M. Wells, The properties of thulium vanadate – An example of molecular field behaviour. *Solid State Commun.* **10**, 265–268 (1972).
14. B. Bleaney, M. R. Wells, Radiofrequency studies of $TmVO_4$. *Proc. R. Soc. Lond. Ser. A Math. Phys. Sci.* **370**, 131–153 (1980).
15. P. Massat *et al*., Field-tuned ferroquadrupolar quantum phase transition in the insulator $TmVO_4$. *Proc. Natl. Acad. Sci. U.S.A.* **119**, e2119942119 (2022).
16. M. Zic, Data repository for Electro-nuclear quantum phase transition in $TmVO_4$. Stanford Digital Repository. https://purl.stanford.edu/ky369kj8044. Deposited 14 September 2025.
17. B. Daudin, B. Salce, S. Smith, Specific heat and thermal conductivity of $TmVO_4$ and $DyVO_4$ with an applied magnetic field. *Le J. Phys. Colloq.* **42**, C6–277 (1981).
18. P. J. Becker, M. J. M. Leask, R. N. Tyte, Optical study of the cooperative Jahn-Teller transition in thulium vanadate, $TmVO_4$. *J. Phys. C Solid State Phys.* **5**, 2027–2036 (1972).
19. P. Hollister, *Ultrasonic Studies of the Jahn-Teller Effect in a Model System* (ProQuest Information and Learning, Ann Arbor, Michigan, 2023).
20. U. Karahasanovic, J. Schmalian, Elastic coupling and spin-driven nematicity in iron-based superconductors. *Phys. Rev. B* **93**, 064520 (2016).
21. Y. Qi, C. Xu, Global phase diagram for magnetism and lattice distortion of iron-pnictide materials. *Phys. Rev. B* **80**, 094402 (2009).
22. H. V. Löhneysen, A. Rosch, M. Vojta, P. Wölfle, Fermi-liquid instabilities at magnetic quantum phase transitions. *Rev. Mod. Phys.* **79**, 1015–1075 (2007).
23. I. Kovacevic *et al*., Probing strongly hybridized nuclear-electronic states in a model quantum ferromagnet. *Phys. Rev. B* **94**, 214433 (2016).
24. R. D. McKenzie, P. C. E. Stamp, Thermodynamics of a quantum Ising system coupled to a spin bath. *Phys. Rev. B* **97**, 214430 (2018).
25. H. M. Rønnow *et al*., Quantum phase transition of a magnet in a spin bath. *Science* **308**, 389–392 (2005).
26. J. Knapp *et al*., Electronuclear transition into a spatially modulated magnetic state in $YbRh_2Si_2$. *Phys. Rev. Lett.* **130**, 126802 (2023).
27. D. H. Nguyen *et al*., Superconductivity in an extreme strange metal. *Nat. Commun.* **12**, 4341 (2021).
28. E. Schuberth *et al*., Emergence of superconductivity in the canonical heavy-electron metal $YbRh_2Si_2$. *Science* **351**, 485–488 (2016).
29. K. Andres, Combined electron-nuclear magnetic-ordering phenomena in singlet-ground-state systems. *Phys. Rev. B* **7**, 4295–4300 (1973).
30. O. Iwakami *et al*., Magnetic ordering of hyperfine-coupled nuclear and 4*f*-electron moments in the clathrate compound $Pr_3Pd_{20}Ge_6$. *Phys. Rev. B* **90**, 100402 (2014).
31. L. Steinke *et al*., Role of hyperfine coupling in magnetic and quadrupolar ordering of $Pr_3Pd_{20}Si_6$. *Phys. Rev. Lett.* **111**, 077202 (2013).
32. J. A. Griffin, M. Huster, R. J. Folweiler, Critical behavior of the spontaneous magnetization at marginal dimensionality in $LiHoF_4$. *Phys. Rev. B* **22**, 4370–4378 (1980).
33. H. Eisenlohr, M. Vojta, Limits to magnetic quantum criticality from nuclear spins. *Phys. Rev. B* **103**, 064405 (2021).
34. H. Ishii, Nuclear magnetism in Van Vleck metals. *J. Low Temp. Phys.* **135**, 579–620 (2004).
35. K. Andres, E. Bucher, J. P. Maita, A. S. Cooper, Observation of cooperative nuclear magnetic order in $PrCu_2$ below 54 mK. *Phys. Rev. Lett.* **28**, 1652–1655 (1972).
36. J. Babcock, J. Kiely, T. Manley, W. Weyhmann, Nuclear magnetic ordering in $PrCu_6$. *Phys. Rev. Lett.* **43**, 380–383 (1979).
37. M. Kubota, H. R. Folle, C. Buchal, R. M. Mueller, F. Pobell, Nuclear magnetic ordering in $PrNi_5$ at 0.4 mK. *Phys. Rev. Lett.* **45**, 1812–1815 (1980).
38. H. Suzuki *et al*., Enhanced nuclear cooling and antiferromagnetism in $HoVO_4$. *J. Phys. Colloq.* **39**, C6–800–C6-802 (1978).
39. H. Suzuki, T. Inoue, Y. Higashino, T. Ohtsuka, Enhanced nuclear cooling and spin-lattice relaxation time in $TmVO_4$. *Phys. Lett. A* **77**, 185–188 (1980).
40. R. Feigelson, Flux growth of type RVO_4 rare-earth vanadate crystals. *J. Am. Ceram. Soc.* **51**, 538–539 (1968).
41. S. Smith, B. Wanklyn, Flux growth of rare earth vanadates and phosphates. *J. Cryst. Growth* **21**, 23–28 (1974).
42. N. Mizutani, H. Suzuki, Magnetic thermal boundary resistance between enhanced nuclear spin system and liquid ^3He. *J. Low Temp. Phys.* **86**, 231–256 (1992).